Overcoming the Transport Limitations of Photopolymer-Derived Architected Carbon

Kjetil Baglo,* Marco Sauermoser, Markus Lid, Thomas Paschke, Abdulla Bin Afif, Markus Lunzer, Andreas Flaten, Martin Steinert, Robert Bock, and Jan Torgersen*

Photopolymer derived carbon grows in popularity, yet the range in available feature sizes is limited. Herein, the focus is on expanding the field to low surface to volume ratio (SVR) structures. A high temperature acrylic photopolymerizable precursor with FTIR and DSC is described and a thermal inert-gas treatment is developed for producing architected carbon in the mm scale with SVR of 1.38×10^{-3} μm^{-1}. Based on thermogravimetric analysis and mass spectrometry, two thermal regimes with activation energies of ≈ 79 and 169 kJ mol^{-1} are distinguished, which is reasoned with mechanisms during the polymer's morphologic conversion between 300 and 500 °C. The temperature range of the major dimensional shrinkage (300–440 °C, 50%) does not match the range of the largest alteration in elemental composition (440–600 °C, O/C 0.25–0.087%). The insights lead to an optimized thermal treatment with an initial ramp (2 °C min^{-1} to 350 °C), isothermal hold (14 h), post hold ramp (0.5 °C min^{-1} to 440 °C) and final ramp (10 °C min^{-1} to 1000 °C). The resulting carbon structures are dimensionally stable, non-porous at the µm scale, and comprise an unprecedented variation in feature sizes (from mm to µm scale). The findings shall advance architected carbon to industrially relevant scales.

1. Introduction

Pyrolysis derived carbon material from photo polymeric precursors that preserves its predefined shape is linked to the field of architected carbon.[1] This field is currently gaining momentum for creating novel electrode designs, for carbon microelectromechanical systems (MEMS), for nanostructures with exceptional mechanical properties, AFM tips and X-ray optical lenses.[1–8] The rapidly growing number of publications and applications in the field signify the great potential of this research. However, the reported structures are yet limited by their amenable range of feature sizes ranging from 160 µm to 200 nm.[1,9,10] The carbonization of polymers is said to be limited by the diffusion of exiting species. The diffusion limitation is expected to increase with an increase in transport distance and the boundary conditions which determine the degrees of freedom in transport directions. In this sense the term "feature size" and "surface to volume ratio (SVR)" is used to describe the transport distance and its degrees of freedom in this work. Although photopolymeric systems have been investigated intensively for their suitability as architected carbon precursor materials, the role of the pyrolysis process itself for obtaining larger dimensional features has been overlooked.[9,11] Some preliminary work has been done in the field of carbon MEMS already back in 2013, addressing feature sizes in the single digit µm dimension.[11] Martinez-Duarte divides the carbonization process into two main stages; in the first stage between 300 and 500 °C, in which hetero atoms get eliminated and a conjugated network forms. In the later stage between 500 and 1200 °C, non-carbon atoms are fully removed and

K. Baglo, A. Flaten, J. Torgersen
Chair of Materials Science
Department of Materials Engineering
TUM School of Engineering and Design
Technical University of Munich
Boltzmannstraße 15, 85748 Garching bei München, Bavaria, Germany
E-mail: kjetil.baglo@tum.de; jan.torgersen@tum.de

M. Sauermoser, M. Lid, A. B. Afif, M. Steinert
Department of Mechanical and Industrial Engineering
Norwegian University of Science and Technology
Richard Birkelands vei 2B, Trondheim, Sør Trøndelag 7491, Norway

T. Paschke
TA Instruments
Waters LLC
Altendorfstr. 10, 32609 Hüllhorst, Nordrhein- Westfalen, Germany

M. Lunzer
Materials Development
UpNano GmbH
1030 Vienna, Modecenterstrasse 22/D36, Austria

R. Bock
Safety of Gas Storage Systems
Federal Institute for Materials Research and Testing (BAM)
12205 Berlin, Unter den Eichen 87, Germany

ADVANCED
SCIENCE NEWS

www.advancedsciencenews.com

**ADVANCED
MATERIALS
TECHNOLOGIES**

www.advmattechnol.de

the aromatic content increases.[3] The existence of these regimes are supported by findings from other fields, such as carbon fiber production.[12] However, little has been reported on the mechanistic effects said to dominate the process, particularly related to the geometry and impact of feature sizes. Natu et al. carbonized UV lithography derived SU-8 pillar structures of different dimensions and geometries and found that the architecture significantly impacts shrinkage during carbonization.[13] Empirical relations were given that relate feature sizes to dimensional shrinkage, yet the mechanism by which this occurs was not described. Rezaie et al. investigated the suitability of five different commercial polymers to produce a architected carbon electrodes with 160 µm thick features.[9] They found that a highly temperature stable formulation was best suited for obtaining dimensionally stable, highly porous carbon electrodes and stated that the degassing of volatiles limits the achievable feature size.

In conventional glassy carbon production, diffusional transport of volatiles through the converting polymer matrix during carbonization is said to set the upper bound of non-porous feature sizes.[14,15] This is linked to the transport distance and the degrees of freedom in transport directions within the polymeric feature.[16] In the field of architected carbon, the SVR is in the range of 1.5 to 0.01 µm^{-1}, with only highly porous architectures achieved for the lowest SVR thus far.[1,9,17,18] To address the demand within electrode production and to benefit from architected carbon in other fields, researchers point out the need for a greater span of feature sizes. Leveraging from the existing knowledge in carbon fiber and glassy carbon production, we believe that the necessary progress in this field can emerge from a better understanding and control of the carbonization process, which we aim to address in this study.

Here, we first investigate the composition and mechanical properties of a commercial high temperature photopolymer. Then we study the effects of the heating rate and isothermal holds in the temperature program used to carbonize two-photon polymerized (2PP) architectures. Further, we explore the kinetics and the nature of ongoing processes during carbonization. Using iso-conversional kinetic analysis, we determine the apparent activation energy and discuss its relation to the diffusional transport of volatiles. The composition of the derived carbon material and the dimensional shrinkage are investigated by energy dispersive X-ray spectroscopy (EDS) and scanning electron microscopy (SEM), and interpreted with respect to the temperature program employed. The insights gained allow us to create a dimensionally stable architecture of significant volume as well as varying feature dimensions within one part. The suitability of an acrylic precursor (UpCarbon) for architected carbon production is demonstrated, and the mechanism of degradation is discussed. The mm scale features achieved in this study, to the best of our knowledge, exceeds those reported in the literature by a factor of ten, making architected carbon accessible and more relevant for fields where large features are required.

2. Results and Discussion

2.1. Choice and Characterization of the Precursor

The number of polymeric precursors suitable for pyrolytic carbon production is vast, with some authors stating that almost any polymer could be converted into a carbon material.[19] When it comes to the carbonization of free-standing polymer structures, the choice of precursor becomes limited. Not only must it decompose in such a manner that carbon material remains, but it also needs to retain its dimensional stability. These prerequisites make thermosets the best-suited precursors as thermoplastic materials tend to melt before they degrade. In this work, precursor refers to the polymer used to obtain the architected carbon. There are several fields working on the production of carbon from organic precursors and the morphology of the precursor differs depending on the application.[3,12,15] It is known from the degradation of organic compounds that a low hydrogen content in combination with high aromaticity and in particular multi-substituted aromatic compounds are good charge generators.[20] The system used in this work is a commercial acrylate-based photopolymer (UpCarbon) developed for architected carbon production and vat polymerization. It has been designed with a high aromatic content as well as a high carbon to oxygen and high carbon to hydrogen ratio, while still allowing for vat polymerization as the patterning technique. The material can be processed either by stereolithography (SLA), digital light processing (DLP), or two-photon polymerization (2PP) depending on the photoinitiator and additives used.[21]

2.1.1. Composition of the Precursor

The Fourier transform infra-red (FTIR) spectrum for the UpCarbon Clear resin and photopolymerized UpCarbon are shown in Figure S1, Supporting Information with spectral details found in Table S1, Supporting Information. The monomer blend is highly aromatic and based on acrylate functional groups. It consists of a blend of mono- and difunctional aromatic compounds. The UpCarbon formulation should be well suited for carbonization as a high aromaticity and unsaturated bonds are reported to promote stable pyrolysis, while the lack of long spacer units or pending side chains is intended to mitigate mass and hence volume shrinkages in the course of carbonization.[19]

2.1.2. Workflow and Choice of Sample Geometry

The workflow chosen to produce the samples was vat polymerization of predefined CAD geometries. There is a trend of leveraging on the geometric freedom 3D printing offers and by utilizing such a technique we demonstrate that carbon also can play an important part as an additive manufacturing material at the macro scale. **Figure 1** shows the workflow for the production process of architected carbon used in this work, as well as 3D illustrations of sample geometries. It is common to use a stabilization step in oxygen for thinner structures like carbon fibers, however in this study no such step was taken in order to mitigate potential differences in the bulk and subphase material of the samples which may arise from the diffusion limitations of the stabilization process.[22]

The sample geometry has a significant impact on the carbonization protocol and the expected dimensional stability.[13] In this study, three sample geometries were chosen to investigate the effects of the temperature program, namely a simple cubic
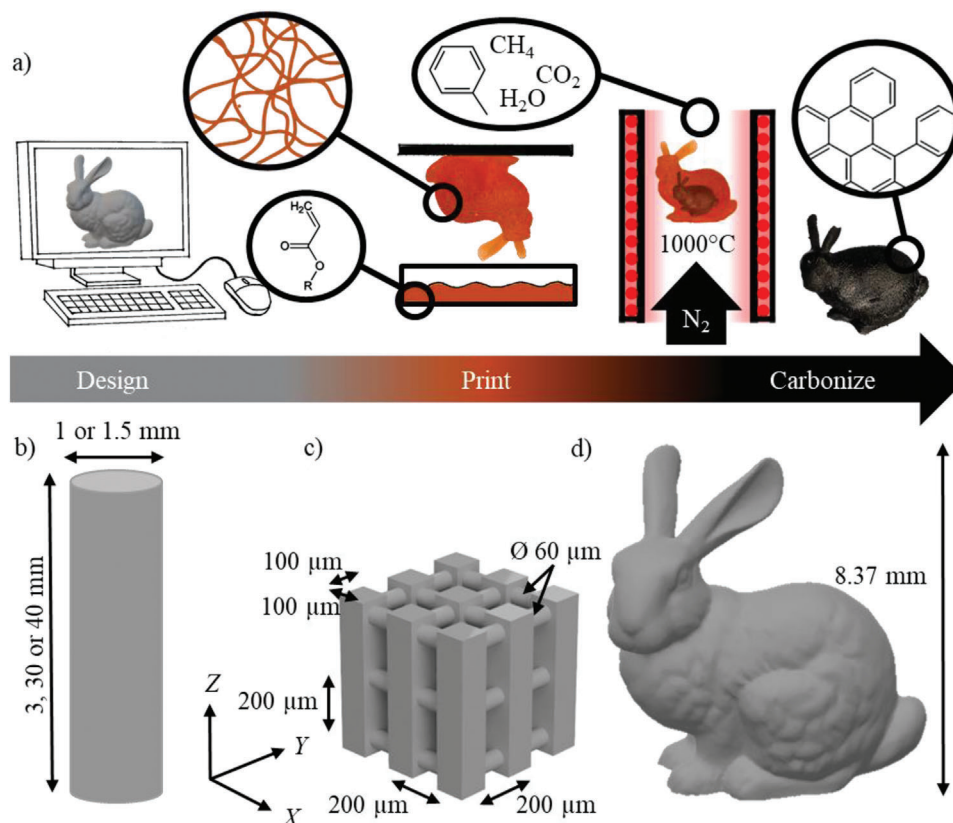
Figure 1. a) Workflow for producing architected carbon structures. After creating the desired structure by computer aided design (CAD), it is fabricated from the acrylic photopolymer by 3D printing using either digital light processing (DLP) or two-photon polymerization (2PP). The polymer part is then carbonized in inert atmosphere, resulting in a shrunken geometry comprised of a carbon allotrope. CAD models of b) rod, c) simple cubic lattice (SCL), and d) rabbit used in the experiments presented in this work. The rods and SCLs were fabricated using 2PP, whereas the rabbit was produced by DLP.

lattice (SCL), single cylindrical rods with 1.0 and 1.5 mm in diameter and lengths of 30 and 40 mm, as well as a rabbit model (Figures 1b–d). These structures were selected for their large span in SVR. The lattice was printed via two-photon polymerization (2PP) using a low magnifying 5× objective (NA 0.25). The overall size of the 2PP printed lattice was 20 mm in the length–width plane and 0.8 mm in the height direction, with a pitch of 200 μm in all three directions, 60 μm strut width in the XY-plane and a 100 μm strut width in the Z-direction (Figure 1c). The simple cubic lattice was designed with thicker struts oriented in the Z-direction to support the structural stability during carbonization. These thicker struts also help reveal any geometry dependent shrinkage, as other work suggests that the distance chemical species emerging in the course of degradation need to traverse effects the shrinkage.[13] The SCL with feature sizes of 60 and 100 μm and calculated SVR of 0.041 μm^{-1}, not including edge effects, were used as the starting point for our investigations as this is comparable to the current state of the art in architected carbon lattices.[9] The rods had a feature size of 1 and 1.5 mm, a length of 3, 30, and 40 mm, with a respective SVR of 4.7×10^{-3}, 4.1×10^{-3}, and 2.7×10^{-3} μm^{-1} for the 1 mm feature size, thus exceeding the state of the art by almost one order of magnitude in SVR. For the thermogravimetric experiments performed, the SCL served as starting point, since structures with comparable SVRs have been demonstrated earlier.[9] The rods were used to

investigate the effect of an increase in transport distance. If the process of carbonizing photopolymers is limited by the transport of volatiles then a larger transport distance will make this limitation more apparent. When developing and investigating the thermal program, the approach was to start with the SCL to find the crucial steps and then fine-tune the process using the rods with a much smaller SVR. Last, a model of a rabbit with a large span in feature sizes was used to demonstrate the capabilities of the precursor temperature program combination presented.

2.1.3. Mechanical Properties of the Precursor

For thermoset polymers, the transport of chemical species emerging in the course of degradation is dependent on the mechanical properties of the material. The largest change in the transport rate occurs at the transition from glassy to rubbery state (T_g).[16] Differential scanning calorimetry (DSC) is used to estimate the T_g, with the results from the DSC of 2PP UpCarbon heated at 5, 10, and 20 °C min^{-1} from 35 to 320 °C shown in Figure S2, Supporting Information. The T_g was estimated at half the heat capacity increase in accordance with ISO 11357-2, and was found to be ramp dependent; 93.3, 99.7 and 100.4 °C for 5, 10, and 20 °C min^{-1}. The polymer is in the rubbery state at the relevant carbonization temperatures, as the onset of thermal

**ADVANCED
SCIENCE NEWS**

www.advancedsciencenews.com

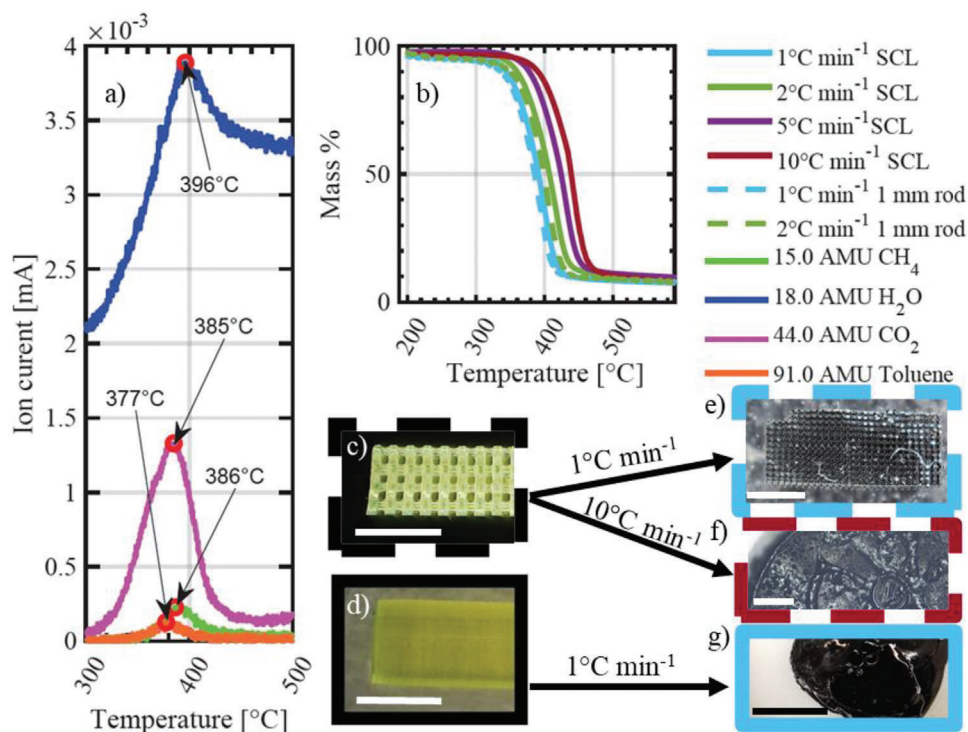**ADVANCED
MATERIALS
TECHNOLOGIES**

www.advmattechnol.de

Figure 2. a) Mass spectrum of the gas fraction of an SCL fragment heated at 5 °C min⁻¹. The temperatures at which the maximum abundance of the detected volatiles occur are denoted with red circles. b) Thermogravimetric analysis (TGA) of four simple cubic lattices (SCL) and two rods. The mass percentage versus temperature at four different heating rates from 25 to 600 °C and two sample geometries of 2PP printed UpCarbon are displayed. c) SCL prior to carbonization. d) 1 mm rod prior to carbonization. e) SCL after a 1 °C min⁻¹ heating rate. f) pitch like residue resulting from a 10 °C min⁻¹ heating rate of a SCL. g) Pitch like residue of a 1 mm rod heated at 1 °C min⁻¹. Subfigure (c–f) illustrates how the process is sensitive to heating rate and scale. All scale bars are 1 mm.

degradation for acrylic polymers is 250 °C.[23] The T_g is therefore much lower than the relevant carbonization temperatures and the effects of increasing diffusion constant should be small. In this state, diffusion is reported to obey Fick's law.[16]

The degree of crosslinking was estimated by Flory's rubber elasticity theory to 1.2×10^3 mol m⁻³ using the dynamic mechanical analysis (DMA) provided in Figure S3, Supporting Information. The degree of crosslinking for photopolymers depends on the temperature and light exposure during patterning and may vary for different processes, especially when considering that 2PP has a very high conversion compared to the more widely used DLP based printers which often require additional post curing steps.[21]

A low stiffness resulting from improper curing can result in the structure deforming under its own weight or by the transport of un-polymerized monomer, provided the polymerization is not thermally activated prior to this. Another aspect to consider is the relation between storage and loss modulus during degradation, as both of them drop upon heating of the UpCarbon Polymer. A decrease in loss modulus is associated with less internal resistance in the material, which again can be associated with improved transport of exiting species due to an increase in free volume.[16] On the other hand, the storage modulus of the polymer is dropping and may cause deformations. We therefore hypothesize that the stiffness of the polymer is a key property to tune to get optimum results during carbonization.

2.2. Effects of the Thermal Program

Using the sample geometries described, the observed effects of the temperature program on the conversion to a carbon allotrope will now be presented. The effects of the temperature program are studied using thermogravimetric analysis (TGA) of the SCL and rod samples.

2.2.1. Effect of Heating Rate and Transport Distance

The simplest approach for a temperature program described in literature is a single step constant heating rate used in carbon microelectromechanical systems (C-MEMS) production, which will be the starting point for our exploration.[11] **Figure 2** shows the relative mass loss of four SCL cut sections heated from 25 to 600 °C at rates of 1, 2, 5, and 10 °C min⁻¹, and the relative mass loss of two cylindrical rods with a diameter of 1 mm and length 3 mm heated at rates of 1 and 2 °C min⁻¹. A mass loss of ≈3% for the SCLs has been observed at 120 °C and 5% for the rods at 180 °C, respectively. This is attributed to the evaporation of non-network constituents released when the material is undergoing glass transition. The major mass loss is 86% to 88% recorded between 280 and 500 °C, followed by a low mass loss of 1 to 2% from 500 to 600 °C. The large mass loss shifts to higher temperatures with a higher heating rate, this was attributed to the thermal lag.
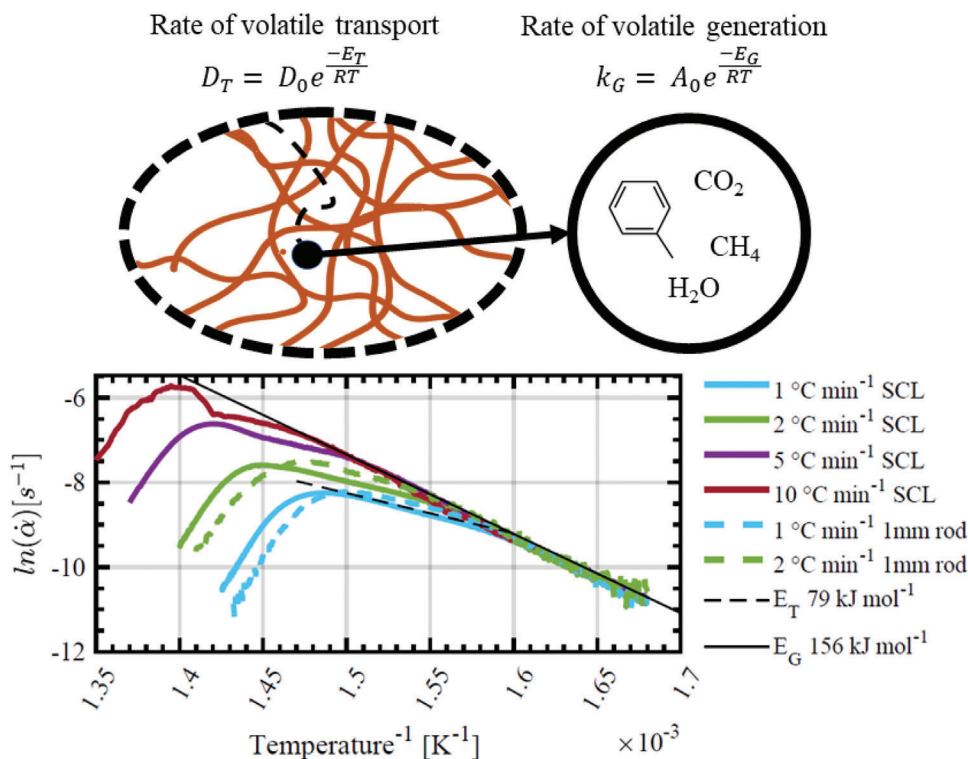
Rate of volatile transport
$$D_T = D_0 e^{\frac{-E_T}{RT}}$$

Rate of volatile generation
$$k_G = A_0 e^{\frac{-E_G}{RT}}$$

Figure 3. Schematic representation of the polymer network and the generated volatiles illustrating how the rate of degradation and subsequent generation of volatiles is limiting the conversion at lower temperatures, below 350 °C (1.6×10^{-3} [K^{-1}]) for a 1 °C min^{-1} heating rate, and the transport of said volatiles at higher temperatures. This hypothesis is supported by the Arrhenius plot showing the natural logarithm of the conversion rate from the thermogravimetric data presented in Figure 2, versus the inverse temperature. The change between the two linear regimes with their estimated activation energies of 156 and 79 kJ mol^{-1} are believed to be caused by a change in the limiting process. The two equations given in the figure describe how the rate of transport, diffusion constant D_T, and rate of volatile generation k_G change with temperature. The activation energies determine the rate dependency of transport and volatile generation. The pre-exponential factors describe how frequently the transport and reactions take place, respectively.

When comparing the rods and SCLs, degradation occurs earlier for the rods, with the inflection point for the rods heated at 1 and 2 °C min^{-1} recorded at 394.25 and 404.82 °C, and for the SCLs at 399.16 and 417.6 °C, respectively. This indicates degradation kinetics that are sensitive to size, with accelerated degradation rate for larger structures. The SCLs heated at 1 and 2 °C min^{-1} produced dimensionally stable structures with a shrinkage of 38.6% and 7% residual mass and 39.8% shrinkage and 9.2% residual mass, respectively. All other samples degraded and produced a film of solidified tar-like material on the inner surfaces of the crucible (Figures 2f,g). This highlights the problem at hand, the process is much more forgiving for short transport distances.

As the gas fraction generated during the degradation provides insight to the degradation mechanism, it was analyzed by online MS. Figure 2a shows the ion current for selected mass traces and total mass fraction versus temperature for an SCL heated from 300 to 500 °C at a rate of 5 °C min^{-1}. The full spectrum is provided in Figure S4, Supporting Information, and the TGA data can be found in Figure S5, Supporting Information. Water, carbon dioxide, methane, and toluene are the main degradation products. The 91 AMU trace is plotted for toluene as it has the highest ion current for this species and 15 AMU for methane to prevent ambiguity with oxygen traces at 16 AMU. The presence of toluene is consistent with the suspected mono-substituted aryl group from the FTIR analysis, as the toluene side chain is easily

removed from the acrylic backbone.[24] The majority of volatile species generated are simple gasses, such as CO_2, H_2O and CH_4, whose diffusive behavior has been studied for a wide range of polymers.[25]

The Friedman method was used to estimate the apparent activation energy for the degradation processes at the heating rates presented.[26] **Figure 3** shows the natural logarithm of the conversion rate versus the inverse temperature (K^{-1}) for the samples ramped from 25 to 600 °C. The activation energy estimated using this approach is a weighted sum of all the activation energies associated with the reactions or transport phenomena. A short introduction to this is provided in the supporting information.

There are two distinct linear regimes observable in Figure 3, one in the range of 322 °C (1.68×10^{-3} K^{-1}) to 352 °C (1.60×10^{-3} K^{-1}) for all samples, and one that starts at higher temperatures. The transition between those regimes depends on the heating rate, where samples undergoing lower heating rates seem to experience this transition at quasi-static conditions. We estimate the activation energy for the lower temperatures with a linear fit of the data points from all six samples, providing us with an apparent activation energy of 156 kJ mol^{-1}. The apparent activation energy for the higher temperatures is estimated using a linear fit in the respective ranges above the transition point. The 10 °C min^{-1} sample represents a special case, since no such upper linear regime could be detected and is hence left out from this as-
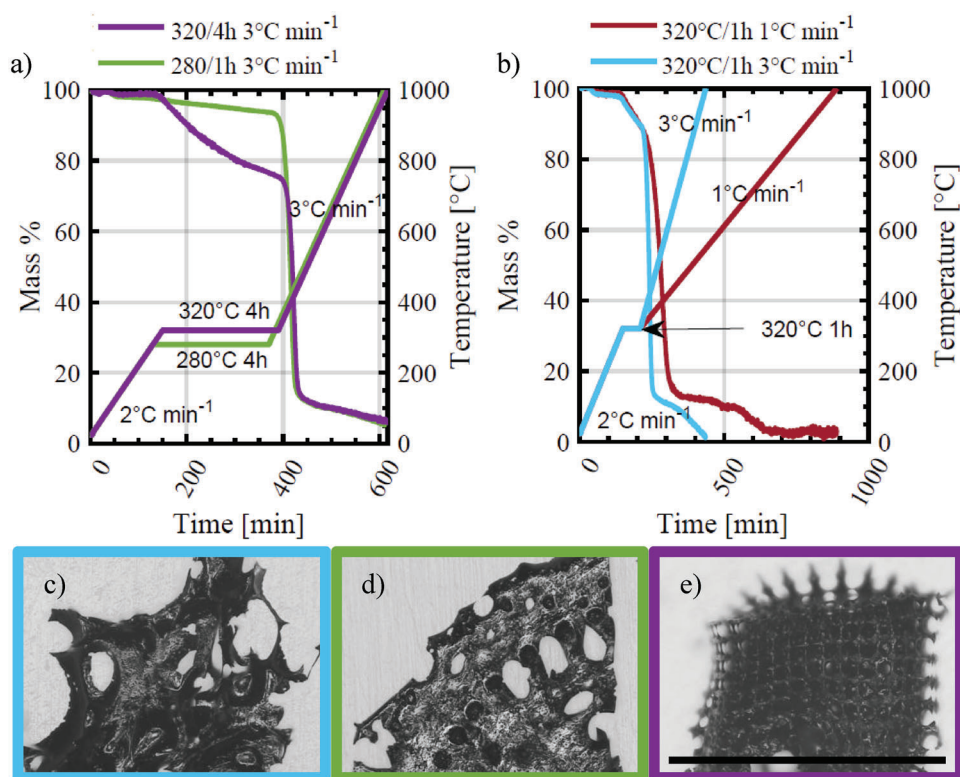
**ADVANCED
SCIENCE NEWS**

www.advancedsciencenews.com

**ADVANCED
MATERIALS
TECHNOLOGIES**

www.advmattechnol.de

Figure 4. TGA mass and temperature program for simple cubic lattices (SCL) treated with a) two different post hold ramps (1 and 3 °C min^{-1}), the slow 1 °C min^{-1} post hold ramp yielded no structure, b) for two different isothermal temperatures (280 and 320 °C). Light microscopy images of c) sample 320/1 h 3 °C min^{-1} with 11% weight loss prior to the post hold ramp, d) sample 280/4 h 3 °C min^{-1} with 4% weight loss prior to the post hold ramp, and e) sample 320/4 h 3 °C min^{-1} with 23% weight loss prior to the post hold ramp, scale bar 1 mm for all images. The dimensional stability of the resulting structure increases with the thermal budget spent in the reaction limited regime.

sessment. The apparent activation energy evaluated similarly to the lower temperature ranges provides us with an estimation of 79 kJ mol^{-1} for this range independent from the ramp.

The square error, 95% confidence bound, thermal range, and fitted values are given in Table S2, Supporting Information. From the MS of an SCL heated at 5 °C min^{-1} (Figure 2a), it is shown that most of the volatiles generated seem to be simple gasses, such as CO_2 and CH_4, where expected activation energies are reported between 10 and 100 kJ mol^{-1}.[25] This is lower than the estimated 156 kJ mol^{-1} for the lower temperature ranges. We therefore hypothesize that this activation energy is related to the degradation of the polymer. Others reported degradation mechanisms of similar (meth)acrylic polymers with activation energies as high as 276 kJ mol^{-1}.[27] Furthermore the limitations caused by diffusive transport and its ties to the crosslinking density is reported to play a vital role in the degradation of (meth)acrylic polymers.[28]

In the conversion process, it seems that degradation and volatile production is the rate limiting factor at lower temperature and not the diffusion rate of the produced volatiles. In the transition between the regimes, the activation energy of the process becomes lower. As we are measuring weight loss in the TGA, we can argue that another process is limiting weight loss above this temperature range. Interestingly, the activation energy is now in a regime that corresponds to the 10 to 100 kJ mol^{-1} range, which, as reported elsewhere, can be correlated to the transport of simple gasses.[25,28] We hence believe that when overcoming this critical

temperature, we are switching to a process that is transport limited, as illustrated in Figure 3.

2.2.2. Effect of Isothermal Hold and Post Hold Heating Rate

We now want to explore an isothermal hold time close to the transition between the explored regimes in the previous experiment. The onset of degradation is within 280 and 320 °C. The effect of an isothermal hold step in this temperature regime together with different ramps past this hold was investigated. We varied hold time, hold temperature, and post hold ramp, with a fixed initial ramp of 2 °C min^{-1} and fixed final temperature of 1000 °C. Initially the post hold ramp was set to 3 °C min^{-1}. The Arrhenius behavior of the conversion rate combined with the time spent at a given temperature is referred to as thermal budget. It is used to describe the thermal energy received and captures the behavior that a long duration at a low temperature can have the same result as a short duration at a higher temperature when evaluating the polymer's conversion to carbon. Cut sections of the SCL were used for this experiment.

Figure 4 shows a selection of TGA data, with the resulting structures. We observe a significant effect on the weight loss rate with the set hold temperature during the isothermal step, where, as expected, a higher temperature results in a higher weight loss rate (Figure 4a). At 280 °C, the weight loss from the isothermal

**ADVANCED
SCIENCE NEWS**

www.advancedsciencenews.com

**ADVANCED
MATERIALS
TECHNOLOGIES**

www.advmattechnol.de

step was only 4% prior to the post hold ramp for a sample held at 4 hours, whereas when held at 320 °C for the same amount of time (4 h), the weight loss was 23%. Also, the dimensional stability is visibly improved (Figures 4d,e). The hold duration also has an effect. At 320 °C, an increase of the hold time from 1 to 4 h increased the dimensional stability visibly (Figures 4c,e). The degree of conversion prior to the post hold ramp is lower for the samples with the low hold time and hold temperature, a greater mass loss therefore has to occur during the 3 °C min^{-1} post hold ramp, this we have also oberved in the previous experiment. It is likely a result of a transport limited process.

Another critical aspect is the rate of the post hold ramp. We looked into two different post hold ramps; 1 and 3 °C min^{-1} for all processes explored so far. After a low post hold ramp of 1 °C min^{-1}, no material was left in the crucible. The sample seemed to have converted to a gaseous or condensate state and exited the TGA chamber. A post hold ramp of 3 °C min^{-1} produced carbon-like material independent of the prior processing.

For 1 °C min^{-1} ramps, a reaction occurs that causes a disintegration of the structure in the range between 600 and 1000 °C, even if a dimensional stable structure was obtained in the initial ramping experiment from 20 to 600 °C (Figure 2e). When reviewing the TGA data in Figure 4b of the sample heated at 1 °C min^{-1} from 320 to 1000 °C, we can clearly see a secondary mass loss stage appearing between 650 and 800 °C. A similar secondary mass loss stage can also be seen for the samples heated at 3 °C min^{-1}, however, here a residual mass remains. Reviewing literature in the field of acrylic photopolymer degradation kinetics, we hypothesize that this observation can be linked to the rate of radical recombination due to caging effects.[29,30] A cage is here referred to as the space that confines radicals inside the network. It is stated that radical pair formation upon thermal activation is reversible. The generated radicals initiate chain degradation but only if they first escape the cage. The probability that radical pairs escape from the cage after their formation decreases with crosslinking density (which lowers the radical diffusion rate) and rate of radical generation (increases the density of radicals and leads to radical collision). If both crosslinking density and rate of radical generation is high, the probability of radical recombination is increasing, a process which seems decisive for obtaining stable carbon structures. This is corroborated by findings from the carbonization of other polymers, where it is stated that highly crosslinked polymers are important to obtain high carbon yield.[31,32]

We conclude that a slower initial ramp and/or an isothermal step in the temperature range where the process is limited by the rate of degradation followed by a fast ramp up to 1000 °C is a good strategy to obtain dimensionally stable carbon.

2.2.3. The Effect of Isothermal Hold Temperature and Transport Distance

With the obtained knowledge, we aimed to explore even lower SVRs reverting back to our initial attempts on carbonizing photopolymer rods fabricated with two photon lithography. We attempted to accelerate the transport and degradation kinetics by raising the temperature of the isothermal step. The thermal budget and hold temperature were increased to 340 °C for 24 h,

350 °C for 14 h, and 360 °C for 6 h. The initial heating rate was kept at 2 °C min^{-1}, but an intermediate heating step of 0.5 °C min^{-1} to 440 °C before the final ramping of 10 °C min^{-1} to 1000 °C was added. This intermediate step was added to ensure full conversion of the main degradation reaction before transitioning to the high post hold ramp. The three different hold temperatures were tested using three SCLs and three rods of 1 mm diameter. The resulting structures and the mass loss is plotted in **Figure 5**. No bubble formation was observed, but the rods were less dimensionally stable than their SCL counterparts. A lower hold temperature resulted in a slower weight loss, Figure 5a. An effect on the residual mass is likely, as a hold temperature of 350 °C gave the highest yield across geometries, however, the differences are too small to provide a significant statement. Here, further experimentation is necessary. For a diffusion-limited process, the time needed for the structures to deplete would depend on the transport distance and hence the SVR, such a dependency cannot be observed here. This means that we still need to explore the limiting factor during this stage in the polymer's degradation.

The isothermal process was modeled using Iso-conversional Kinetic Analysis, which is a useful toolbox for investigating the processes described her. The article by Sergey Vyazovkin covers this well and there is a short introduction that can be found in the supporting information.[33] In Figure 5c, the degree of conversion (α) is plotted versus the rate of conversion ($\dot{\alpha}$) for all samples displayed in Figure 5. We find the linear first order reaction model presented the best fit out of the common transport and reaction models.[34,35] The results of the fitting can be found in Figure 5c, and Figure S6, Supporting Information, with the pre-exponential factor A being $e^{23.22}$ and an activation energy E of 167.8 kJ mol^{-1}. Table S3, Supporting Information states the mean value, 95% confidence interval, and R^2 for the fitted values. Comparing the mass loss of the samples to the model, we observe that the first 30 to 40% of the conversion deviates, nevertheless, it captures a good portion of the process. The first order reaction model does not include diffusive behavior. This, together with the observed similarity of the weight loss between SCL and rods, suggests that the process might indeed not be limited by the diffusive transport of gases.

Looking at the thermal degradation of methacrylic systems, Lomakin et al. reports the following processes with corresponding ascending activation energies above 15% weight loss under isothermal conditions.[27] A linear fragment is a fragment of the polymer network originating from the monofunctional polymer constituents while a network fragment is resulting from the multi-functional constituents.

1) Depropagation of linear fragments with effective activation energy of 118 to 124 kJ mol^{-1}, and 74 to 83 kJ mol^{-1} for network fragments.
2) The termination of linear polymer radicals with effective activation energy of 160 to 163 kJ mol^{-1}.
3) The initiation of random chain scission of the C–C backbone with effective activation energy of 215 to 276 kJ mol^{-1}.

Our activation energy estimation of 168.7 kJ mol^{-1} fits very nicely into the described range, however, cannot be ascribed to one reaction only. There is apparently a large amount of processes that have their activation energies in this range including
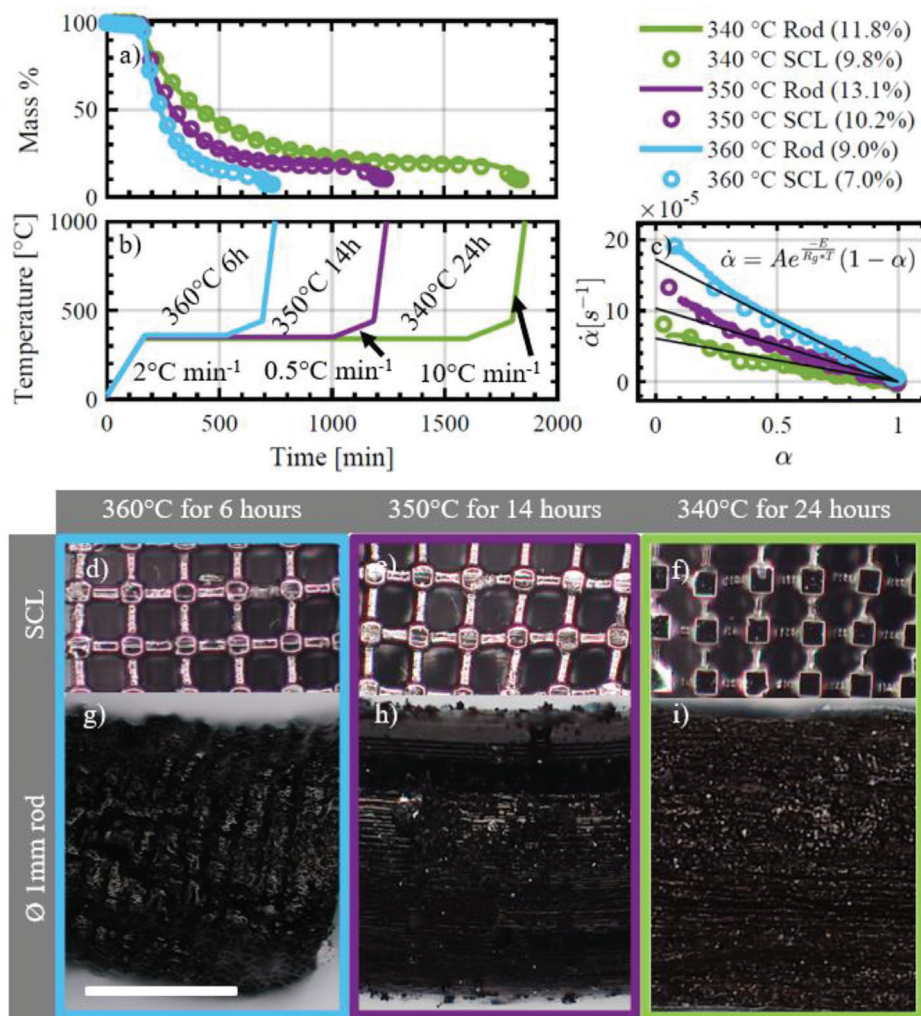
**ADVANCED
SCIENCE NEWS**

www.advancedsciencenews.com

**ADVANCED
MATERIALS
TECHNOLOGIES**

www.advmattechnol.de

Figure 5. a) Weight loss, b) temperature program, and c) conversion plot for the TGA of the three SCLs and the three 1 mm rods undergoing three different isothermal temperature programs, residual mass in parenthesis. d–i) Light microscope images of resulting carbon structures treated at three different hold temperatures, scale bar 200 μm for all samples. There is no difference in depletion time between the SCL and rod samples indicating that the process is not transport limited. This is further supported by the seemingly linear trend in the conversion plot which is indicative of first order reaction kinetics.

diffusive transport of larger molecules.[36] Krongauz reports that the degradation of acrylic photopolymers is determined by the rate of polymer segment rotation leading to decarboxylation and formation of chain segments with consequent formation of cyclic intermediates (cyclization).[29] The formation of volatile species such as CO_2, CH_4 and others are, according to literature, not rate limiting as their diffusion rate is higher. The length of a polymer available for rearrangement, in turn, is dependent on its glass transition temperature and the degree of crosslinking, which we hypothesize, are critical parameters for the suitability of a photopolymer to retain its shape during carbonization. It has to be noted, however, that detached fragments including monomers may also influence the degradation if they do not take part in stabilizing processes such as the formation of cyclic intermediates.

A larger upper bound in feature sizes is further substantiated by literature in the field of carbon production, where non-porous glassy carbon is reported to have an upper transport distance of 4.5 mm prior to carbonization.[14,37] Here, we deal with a 0.5 mm transport distance, which is far from the reported limitation.

2.3. Shrinkage and Composition during Carbonization

The shrinkage and composition at different stages in the temperature program was investigated using EDS of 3 mm long, 1 mm in diameter rods heated to different stages in the temperature program. The average shrinkage in diameter D and length L, and the carbon and oxygen content are summarized in Figure S7 and Table S4, Supporting Information. The largest shrinkage occurs in the 20 to 440 °C temperature range, while the most significant change in oxygen and carbon content occurred between 440 and 600 °C. It seems that the sum of volatiles responsible for the large weight loss and shrinkage observed between 25 and 440 °C have a carbon to oxygen ratio similar to that of the polymer precursor.

**ADVANCED
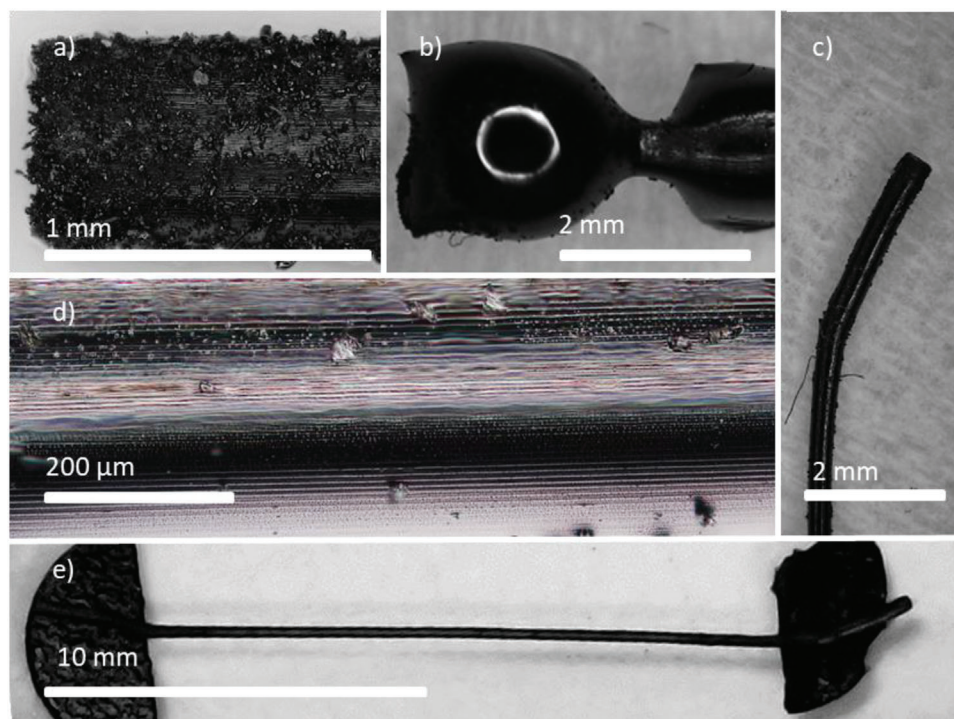SCIENCE NEWS**

www.advancedsciencenews.com

**ADVANCED
MATERIALS
TECHNOLOGIES**

www.advmattechnol.de

Figure 6. a) End of Sample Ø 1 mm 10 h showing pertruding material observed at the end of all samples. b) Sample Ø1.5 mm 14 h presenting with extensive bubble formation likely caused by an excessive hold time. c) End of Sample Ø 1 mm 14 h showing how the ends lift from the substrate during carbonization. d) Sample Ø 1.5 mm 10 h, showing the surface quality achieved in the middle of the rod. e) Sample Ø 1 mm 14 h displaying the overall size and shape of the carbonized samples.

This is consistent with the scission of monomer and cyclification process suggested by Krongauz.[29] Following the published argumentation line, the drastic change in oxygen content between 440 and 600 °C is then likely related to the elimination of oxygen from these cyclic intermediates however this cannot be confirmed by the given data. The SCL held at 340 °C for 24 h and heated to 1000 °C in Figure 5, had a shrinkage in unit cell size of 64% and a shrinkage in thickness of 68%, compared to the rods in Figure S7, Supporting Information, which had a shrinkage of 56% in thickness and 57% in length at 1000 °C. Less shrinkage with a thicker structure is consistent with the proposed degradation mechanisms, as a longer path gives more time for carburizable species to stabilize, for instance through cyclization. This is further supported by the higher residual mass fraction for the thicker structures which can be seen in Figure 5. It is therefore expected that the residual mass and shrinkage will be dependent on the feature size and SVR and will not be constant across geometries.

One argument that could be made regarding the similarity of the weight loss between the SCL and the rods is that the network we produce through this process is porous, which decreases the transport distances. This we want to explore next.

2.4. Porosity of the Obtained Architected Carbon

Further decreasing the SVR, we looked at the carbonization of 30 and 40 mm long circular rods of 1 and 1.5 mm diameter. The protocols employed are summarized in Table S5, Supporting In-

formation, with the 30 and 40 mm long rods held for 10 and 14 h, respectively. There are four observations we can make and are displayed in **Figure 6**.

- First, the ends of the rods, where the surface area is higher, show protruding material independent on the processing conditions, lengths and thicknesses (Figure 6a). However, the main section of the rod appears of high quality with the individual passes of the laser beam causing polymerization along its trace still visible (Figure 6d).
- The length did not have any effect on the carbonization result.
- For the thicker samples with the lower SVR, longer isothermal hold times led to bubble formation, Figure 6b,d shows 1.5 mm rods with 10 and 14 h hold time at 360 °C.
- If the rod is not constrained on the ends, curling can be observed, Figure 6c,e.

The results from a 4-point electrical conductivity measurement of the rods presented in Figure 6, with the exception of sample Ø 1.5 mm 14 h due to the large defects, are presented in Table S6, Supporting Information. The resistivity varied from 0.95×10^{-4} to 1.37×10^{-4} Ωm.

The rods were broken, and the resulting fracture surface was examined using SEM. All samples showed the same type of fracture surface, **Figure 7**. There is no apparent porosity that can be resolved with the SEM, but there is a change in surface texture when inspecting different parts of the fracture surface. Bulk material as seen in Figures 7a–c is grainy but non-porous at the micron scale. The fracture surface seems unlike the one reported
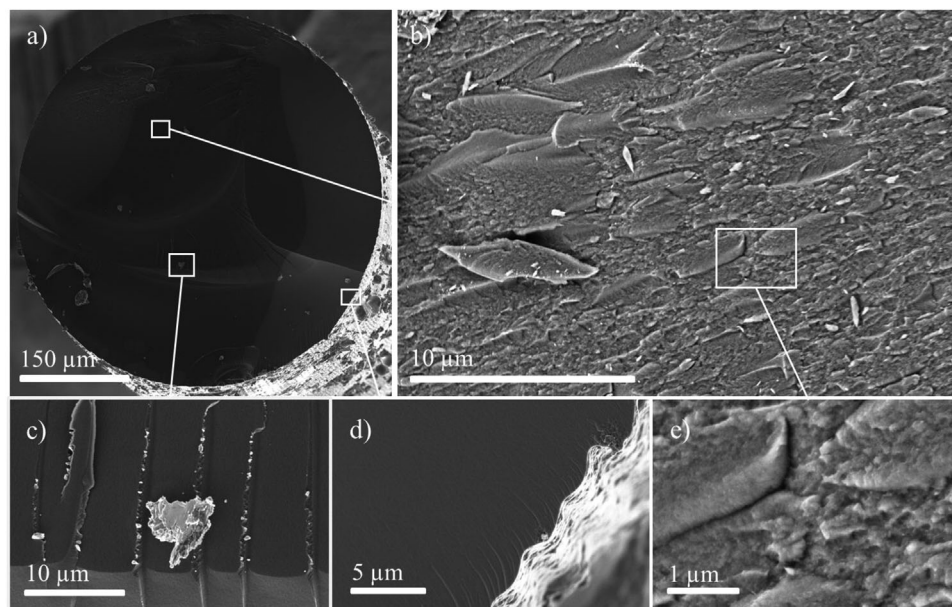
**ADVANCED
SCIENCE NEWS**

www.advancedsciencenews.com

**ADVANCED
MATERIALS
TECHNOLOGIES**

www.advmattechnol.de

Figure 7. Fracture surface of Sample Ø 1 mm 10 h. a) overview of the fracture surface. b) Grainy region of the fracture surface. c) Stepping on the fracture surface. d) Edge of fracture surface. e) Closer view of the grainy region. The material presents as non-porous at the micron scale.

for glassy carbon, which usually has distinct striations or is completely smooth.[37] Figure 7e shows a closer view of the grainy region which could be due to a porosity at the 100 nm scale. This is far from the porosity reported by Rezaei et al. for other acrylic photopolymers undergoing carbonization.[9] This can be related to the different polymer, thermal processing and printing process investigated here. For a detailed comparison further studies involving other formulations are required. Interestingly, the fracture zones close to the surfaces, Figure 7c, in contrast, seem similar to those reported for glassy carbon, which may be indicative that bulk material deviates from the one close to the surface.[37]

2.5. Demonstration of Achievable Scale

Based on the thermal program and the outlined theory, the scale at which architected carbon can be obtained should be much larger than the current state of the art. To explore this, a model of a rabbit, with a height of 8.37 and 127.4 mm³ volume was printed using a digital light processing (DLP) 3D-printer. The resin is based on the same photopolymer mixture as for the 2PP experiments but mixed with a different UV-photoinitiator and UV-absorber.[21] The rabbit had a SVR of 1.38×10^{-3} µm^{-1}, measured from the scaled CAD model.[38] The employed carbonization strategy was 2 °C min^{-1} to 350 °C, hold for 14 h before a 0.5 °C min^{-1} ramp to 440 °C, then 10 °C min^{-1} to 1000 °C. The resulting carbon rabbit is shown in **Figure 8**. Similarly to the experiments with the rod structure, the contour line pattern on the surface of the rabbit caused by the layer-by-layer printing process, is also visible here, despite in much lower resolution due to the nature of the DLP process. Retaining these features through the carbonization demonstrates how well they can be preserved. The rabbit consists of various features vastly differing in their SVR. Interestingly, the overall shape of the rabbit could be preserved with nearly all features intact. However, the shape is somewhat deformed, which might be related to sagging under its own weight. With further optimization on the stiffness of the polymer and an improved understanding of the cyclization behavior during carbonization as well as adaptions to the CAD prior to printing, we hypothesize that quite close resemblance can be obtained.

3. Conclusion

In the presented work, we have investigated and developed a thermal program to carbonize the commercial acrylic photopolymer UpCarbon to architected carbon. After discussing mechanical properties and composition, the effect of heating rate, isothermal hold time and temperature in the thermal treatment was investigated and discussed with respect to the degradation process of the polymer. Two distinct activation energies for the degradation processes were described (79 and 169 kJ mol^{-1}) and discussed with respect to the degradation mechanisms of the polymer. Given the right conditions, the diffusional transport of volatiles is not dominating, but rather the rearrangement rate determined by the mobility of polymer fragments inside the degrading network. A thermal program corresponding to these mechanisms was developed, the program consisted of: 2 °C min^{-1} to 350 °C with an isothermal hold for 14 h, followed by a ramp of 0.5 °C min^{-1} to 440 °C, and last a ramp of 10 °C min^{-1} to 1000 °C. SEM micrographs do not show any porosity at the µm scale and the original geometrical relations are retained. The achieved structures have SVRs of down to 1.38×10^{-3} µm^{-1} and transport distances of several millimeters, which proves that a deeper knowledge of the dimensionally stable carbonization process may indeed enable architected carbon with features from mm to nm scale in one part, at least theroetically . We show that geometrically stable CAD defined carbon structures ranging from 7 mm in thick-
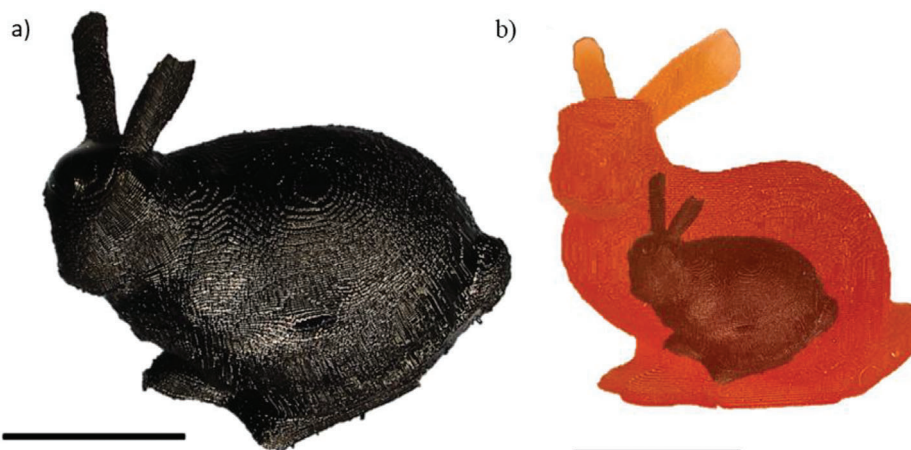
**ADVANCED
SCIENCE NEWS**

www.advancedsciencenews.com

**ADVANCED
MATERIALS
TECHNOLOGIES**

www.advmattechnol.de

Figure 8. a) 3D-printed and pyrolyzed rabbit made from UpCarbon, scale bare 2 mm. b) Carbonized compared to the as printed geometry, scale bar 4 mm. Figure S8, Supporting Information shows the rabbit prior to carbonization. The temperature program utilized is 2 °C min^{-1} to 350 °C, hold for 14 h before a 0.5 °C min^{-1} ramp to 440 °C, then 10 °C min^{-1} to 1000 °C.

Table 1. Printer settings used for the production of 2PP SCL and rod sample geometries.

Object	Object	Scanning speed [mm s^{-1}]	Infill mode	d_{xy} [µm]	d_z [µm]	Laser power [mW]
SCL	5×/0.25	750	Coarse	10	10	250
Rods	4×/0.16	750	Coarse	10	10	350

ness to tens of microns (measured prior to carbonization) in one part can be obtained. We believe that this work can serve as a foundation for utilizing architected carbon in the macroscopic domain.

4. Experimental Section

Materials: 2,4-dihydroxyazobenzene (Sudan Orange G, CAS: 2051-85-6), phenylbis(2,4,6-trimethylbenzoyl) phosphine oxide (BAPO, CAS: 162881-26-7), and acetone were purchased from Sigma-Aldrich (Oslo, Norway) and used without further purification. The commercial two-photon polymerization (2PP) resin UpCarbon was provided by UpNano GmbH (Austria). Additionally, an unmodified base resin formulation of UpCarbon without any two-photon active additives (UpCarbon Clear) was provided.

Two-Photon Polymerization: 2PP 3D printed parts were fabricated using a NanoOne 1000 high-resolution 3D printing system (UpNano GmbH, Austria) in vat mode.[39] Here, the laser (80 MHz repetition rate, 90 fs pulse length, and 780 nm wavelength) was focused through a high-precision cover glass into a material vat containing the resin and maintained at a constant height above the glass window. For layer-wise 3D structuring, the laser was scanned along the *xy* plane by a galvanometer scanner, and the objective together with the vat is lowered along the *z* axis using a piezo stage. A 5× air objective (NA 0.25, Fluar 5×/0,25, Zeiss) and a 4× air objective (NA 0.16, UPlanSApo 4×, Olympus) were used for focusing. Methacrylized borosilicate glass substrates were used.[40] Depending on the objective different laser powers, scanning speeds, line distances (d_{xy}) and layer spacings (d_z) were used (see **Table 1**).

DLP Resin Preparation and Printing: A solution of 2,4-dihydroxyazobenzene (0.005 g) and phenylbis(2,4,6-trimethylbenzoyl) phosphine oxide (1 g) in acetone (20 mL) was prepared at 30 °C by magnetic steering. The solution was mixed with UpCarbon base resin (98.95

g) in a Heidolph rotary evaporator at 150 RPM, 60 °C and atmospheric pressure for 60 min, followed by solvent evaporation at 60 °C and 350 mbar for 5 h. A rabbit was printed on a Way2Production Solflex 650 DLP 3D printer (W2P Engineering GmbH, Austria) placed in a box with an ambient temperature of 60 °C. The rabbit model was downloaded and scaled by a factor of 0.1, then printed with a layer thickness of 50 µm.[38] The printed rabbit is depicted in Figure S8, Supporting Information.

Carbonization: Two instruments were used to carbonize the samples. The SCL and rod sections, with the exception of the eight rods used for EDS, were carbonized using the TGA as described below. The 30 and 40 mm long rods, the eight rods used for EDS, and the rabbit were carbonized using the tube furnace (Carbolite 3508) equipped with a vacuum pump. The eight rods were cut and ground to a length of 3 mm using 800 and then 1200 grit abrasive paper, from a 30 mm rod. The TGA was flushed with Nitrogen for 15 min at 250 mL min^{-1} before all references and tests and the tube furnace was evacuated to a pressure of 10^{-2} Pa and filed with Nitrogen three times before the temperature program was started.

TGA: The thermogravimetric data was recorded using a Netzsch STA 449 C Jupiter with 90 µL alumina crucible. The initial weight of each sample was determined using a lab scale (Mettler AE 163) and analyzed in nitrogen atmosphere with a flow of 20 mL at 0.5 bar overpressure. The lattices used in the analysis was cut using a scalpel to fit a cylindrical 90 µL crucible suited for TGA.

FTIR: The spectrum of UpCarbon Clear monomer blend and polymer was recorded using a Bruker Vertex 80v—FTIR spectrometer. The spectra for the liquid monomer blend was recorded with 1 cm^{-1} sampling rate, and acquisition mode attenuated total reflectance (ATR). The spectra for the 2PP polymerized UpCarbon were recorded using ATR with a sampling rate of 3 cm^{-1}. The powder for the measurement was prepared by crushing a piece of SCL in a glass mortar. The sample stage was cleaned with 96% ethanol in between measurements, and a background was taken in the evacuated empty stage.

DSC: The heat flow was recorded using a TA Instruments Discovery DSC250 with aluminum Tzero hermetic pans and a nitrogen flow of 50 mL min^{-1}. The pan was filled with three Ø 1 mm rods, cut from a 30 mm long sample, weighing a total of 11.3 mg.

DMA: The data for the dynamic mechanical analysis was recorded on a Rheometric Scientific DMTA V with a strain of 0.1%, auto tension with a minimum force of 0.5 N, and a dynamic load oscillating at 10 Hz with an amplitude of 0.4 times the static load.

Mass Spectrometry: MS experiments were performed in a TA Instruments HP-TGA 7500 coupled with a Discovery II quadrupole mass spectrometer. A 3 mg SCL sample was analyzed in a 90 µL alumina cru-

**ADVANCED
SCIENCE NEWS**

www.advancedsciencenews.com

**ADVANCED
MATERIALS
TECHNOLOGIES**

www.advmattechnol.de

cible in 20 mL min^{-1} Argon at 1.5 bar. The mass spectrometer operated in electron impact ionization mode with a mass range of 1–100 amu.

Microscopy: Optical microscope images were taken using a Hirox RH-2000 Digital Microscope with a one to ten times optical zoom and 5×, 10×, and 35× objectives. SEM images were acquired with Thermo Fisher Apreo SEM, with a standard secondary electron detector. The acceleration voltage was 3 kV, and the beam current 50 pA.

Conductivity: The conductivity of the graphitized rods was measured using a FLUKE 8846 A precision multimeter with a custom 4-point probing station. The distance between the probes and the dimensions of the rods were measured using a Hirox RH-2000 Digital Microscope while the conductivity measurements were performed.

EDS: EDS was done with Thermo Fisher Apreo SEM, using X-MAX 80 from Oxford Instruments. The Aztec software compares the emitted spectrum to referenced values to yield the sample composition. For the experiment, a 20 kV beam was used. The samples were made by scraping a section of a few square millimeters on the carbon rod surface with a blade to remove potential thin layers of contamination. The EDS was mapped in this scraped area and averaged to compute a compositional profile in this region.

Supporting Information

Supporting Information is available from the Wiley Online Library or from the author.

Conflict of Interest

The authors declare no conflict of interest.

Data Availability Statement

The data that support the findings of this study are available from the corresponding author upon reasonable request.

[1] K. Narita, M. A. Citrin, H. Yang, X. Xia, J. R. Greer, *Adv. Energy Mater.* **2021**, *11*, 2002637.

[2] D. Niblett, Z. Guo, S. Holmes, V. Niasar, R. Prosser, *Int. J. Hydrogen Energy* **2022**, *47*, 23393.

[3] R. Martinez-Duarte, *Micromachines* **2014**, *5*, 766.

[4] A. Zakhurdaeva, P.-I. Dietrich, H. Hölscher, C. Koos, J. G. Korvink, S. Sharma, *Micromachines* **2017**, *8*, 285.

[5] M. I. Sharipova, T. G. Baluyan, K. A. Abrashitova, G. E. Kulagin, A. K. Petrov, A. S. Chizhov, A. S. Chizhov, T. B. Shatalova, D. Chubich, D. A. Kolymagin, A. G. Vitukhnovsky, A. G. Vitukhnovsky, V. O. Bessonov, V. O. Bessonov, A. A. Fedyanin, *Opt. Mater. Express* **2021**, *11*, 371.

[6] C. M. Portela, B. W. Edwards, D. Veysset, Y. Sun, K. A. Nelson, D. M. Kochmann, J. R. Greer, *Nat. Mater.* **2021**, *20*, 1491.

[7] M. Islam, A. Diaz Lantada, M. Ramos, D. Mager, J. Korvink, *Adv. Eng. Mater.* **2020**, *22*, 2000083.

[8] J. Ye, L. Liu, J. Oakdale, J. Lefebvre, S. Bhowmick, T. Voisin, J. D. Roehling, W. L. Smith, M. R. Cerón, J. van Ham, L. B. Bayu Aji, M. M. Biener, Y. M. Wang, P. R. Onck, J. Biener, *Nat. Mater.* **2021**, *20*, 1498.

[9] B. Rezaei, J. Y. Pan, C. Gundlach, S. S. Keller, *Mater. Des.* **2020**, *193*, 108834.

[10] J. Bauer, A. Schroer, R. Schwaiger, O. Kraft, *Nat. Mater.* **2016**, *15*, 438.

[11] Y. Daicho, T. Murakami, T. Hagiwara, S. Maruo, *Opt. Mater. Express* **2013**, *3*, 875.

[12] M. Al Aiti, D. Jehnichen, D. Fischer, G. Brünig, G. Heinrich, *Prog. Mater. Sci.* **2018**, *98*, 477.

[13] R. Natu, M. Islam, J. Gilmore, R. Martinez-Duarte, *J. Anal. Appl. Pyrolysis* **2018**, *131*, 17.

[14] H. Maleki, L. R. Holland, G. M. Jenkins, R. L. Zimmerman, *Carbon* **1997**, *35*, 227.

[15] V. Uskoković, *Carbon Trends* **2021**, *5*, 100116.

[16] M. H. Klopffer, B. Flaconneche, *Oil Gas Sci. Technol.* **2001**, *56*, 223.

[17] B. Bian, D. Shi, X. Cai, M. Hu, Q. Guo, C. Zhang, Q. Wang, A. X. Sun, J. Yang, *Nano Energy* **2018**, *44*, 174.

[18] Z. Lyu, G. J. H. Lim, J. J. Koh, Y. Li, Y. Ma, J. Ding, J. Wang, Z. Hu, J. Wang, W. Chen, Y. Chen, *Joule* **2021**, *5*, 89.

[19] E. Gottlieb, K. Matyjaszewski, T. Kowalewski, *Adv. Mater.* **2019**, *31*, 1804626.

[20] D. W. V. Krevelen, K. T. Nijenhuis, in *Properties of Polymers*, 4th Ed., Elsevier, Amsterdam **2009**, pp. 763–777

[21] S. C. Ligon, R. Liska, J. Stampfl, M. Gurr, R. Mülhaupt, *Chem. Rev.* **2017**, *117*, 10212.

[22] S. B. Warner, L. H. Peebles, D. R. Uhlmann, *J. Mater. Sci.* **1979**, *14*, 556.

[23] G. Ozaydin-Ince, K. K. Gleason, *J. Electrochem. Soc.* **2010**, *157*, D41.

[24] G. G. Cameron, D. R. Kane, *Polymer* **1968**, *9*, 461.

[25] G. J. Van Amerongen, *Rubber Chem. Technol.* **1951**, *24*, 109.

[26] M. Venkatesh, P. Ravi, S. P. Tewari, *J. Phys. Chem. A* **2013**, *117*, 10162.

[27] S. M. Lomakin, R. M. Aseeva, G. E. Zaikov, *Int. J. Polym. Mater. Polym. Biomater.* **1996**, *31*, 153.

[28] S. M. Lomakin, J. E. Brown, R. S. Breese, M. R. Nyden, *Polym. Degrad. Stab.* **1993**, *41*, 229.

[29] V. V. Krongauz, *Thermochim. Acta* **2010**, *503–504*, 70.

[30] V. V. Krongauz, *J. Therm. Anal. Calorim.* **2019**, *138*, 3425.

[31] S.-H. Kang, K.-W. Kim, B.-J. Kim, *Polymers* **2021**, *13*, 2157.

[32] S. Straus, S. L. Madorsky, *J. Res. Natl. Bur. Stand., Sect. A* **1961**, *65A*, 243.

[33] S. Vyazovkin, N. Sbirrazzuoli, *Macromol. Rapid Commun.* **2006**, *27*, 1515.

[34] K. Chrissafis, *J. Therm. Anal. Calorim.* **2009**, *95*, 273.

[35] H. Mahmood, A. Shakeel, A. Abdullah, M. I. Khan, M. Moniruzzaman, *Polymers* **2021**, *13*, 2504.

[36] F. Welle, *Polymers* **2021**, *13*, 1317.

[37] A. M. Molodets, A. A. Golyshev, A. S. Savinykh, V. V. Kim, *J. Exp. Theor. Phys.* **2016**, *122*, 289.

[38] J. Miller, High Resolution Stanford Bunny, **2021**. https://www.thingiverse.com/thing:11622

[39] M. Lunzer, J. S. Beckwith, F. Chalupa-Gantner, A. Rosspeintner, G. Licari, W. Steiger, C. Hametner, R. Liska, J. Fröhlich, E. Vauthey, A. Ovsianikov, B. Holzer, *Chem. Mater.* **2022**, *34*, 3042.

[40] M. Lunzer, L. Shi, O. G. Andriotis, P. Gruber, M. Markovic, P. J. Thurner, D. Ossipov, R. Liska, A. Ovsianikov, *Angew. Chem., Int. Ed.* **2018**, *57*, 15122.

2300092 (12 of 12)